International Journal of Nanomedicine

Dovepress
Taylor & Francis Group

Open Access Full Text Article

ORIGINAL RESEARCH

Mechanism of a Novel Complex: Zinc Oxide Nanoparticles-Luteolin to Promote Ferroptosis in Human Acute Myeloid Leukemia Cells in Vitro

Wenhao Wang[1,*], Zonghong Li[2,*], Chunyi Lyu[1], Teng Wang[1], Chen Han[1], Siyuan Cui[3], Jinxin Wang[3], Ruirong Xu[3–5]

[1]First Clinical Medical College, Shandong University of Traditional Chinese Medicine, Jinan, People's Republic of China; [2]Department of Hematology, Shandong Cancer Hospital and Institute, Shandong First Medical University and Shandong Academy of Medical Sciences, Jinan, People's Republic of China; [3]Department of Hematology, Shandong University of Traditional Chinese Medicine Affiliated Hospital, Jinan, People's Republic of China; [4]Key Laboratory of Integrated Traditional Chinese and Western Medicine for Hematology, Health Commission of Shandong Province, Jinan, People's Republic of China; [5]Institute of Hematology, Shandong University of Traditional Chinese Medicine, Jinan, People's Republic of China

*These authors contributed equally to this work

Correspondence: Ruirong Xu, Shandong University of Traditional Chinese Medicine Affiliated Hospital, Jinan, 250000, People's Republic of China, Email shandongxuruirong@163.com

Purpose: Acute myeloid leukemia (AML) is a hematological malignancy. Zinc oxide nanoparticles (ZnO NPs) and Luteolin are commonly used to fight cancer. In this study, we synthesized a new complex: zinc oxide nanoparticles-luteolin (ZnONPs-Lut) and aimed to investigate its effects on cell death in the AML cell line (MOLM-13) in vitro and to elucidate the underlying mechanisms.

Methods: We assessed cell viability, quantified changes in gene expression using real-time quantitative PCR (qRT-PCR), and measured changes in ferrous (Fe^{2+}) content, glutathione (GSH) content, malondialdehyde (MDA) content, reactive oxygen species (ROS), and mitochondrial membrane potential (MMP) levels following treatment with different concentrations of MOLM-13 cells with different concentrations of ZnONPs-Lut. Western blotting was used to detect the protein expression levels of ACSL4, GPX4, FTH1, and SLC7A11, while the cell morphology was observed by transmission electron microscopy (TEM). Meanwhile, the effect of Ferrostatin-1 (Fer-1), a ferroptosis inhibitor, on the expression of the aforementioned ferroptosis-related proteins and cell morphology was evaluated.

Results: The results showed that ZnONPs-Lut was able to significantly inhibit the proliferation of MOLM-13 cells in a time- and dose-dependent manner. Additionally, it increased the concentrations of Fe^{2+} and MDA, reduced the expression levels of GSH and MMP, and induced ROS generation. Furthermore, it also enhanced the expression of ACSL4 protein while decreasing the expression of GPX4, FTH1, and SLC7A11 proteins. Notably, Fer-1 was able to significantly restrain the changes in protein levels and mitochondrial morphology damage induced by ZnONPs-Lut after its action on cells.

Conclusion: ZnONPs-Lut inhibits the proliferation of MOLM-13 cells, likely through promoting the cellular ferroptosis signaling pathway. These findings suggest that ZnONPs-Lut could be a potential therapeutic approach for AML.

Keywords: acute myeloid leukemia, ferroptosis, reactive oxygen species, zinc oxide nanoparticles, luteolin

Introduction

Acute myeloid leukemia (AML) is a malignant disease, characterized by the uncontrolled proliferation of bone marrow stem cells. It is associated with infections, anemia, and hemorrhage, with a median age of disease diagnosis of 68 years old.[1,2] In 2024, it is estimated that there will be 20,800 new cases of AML in the United States, and 11,220 people will die from the disease.[3] Although the evolution of emerging therapeutic options, such as targeted therapies and immunotherapies, has played an important role in improving survival rates and quality of life for AML patients, the treatment options for AML patients still remain limited.[4] Drug toxicity, long-term drug resistance, and the slow progress of

Received: 15 December 2024
Accepted: 20 March 2025
Published: 2 April 2025

immunotherapy—due to the scarcity of AML-specific target antigens and low mutation rates—have significantly hindered advancements in AML treatment.[5,6] Up to 50% of patients fail to achieve remission during initial treatment, leading to refractory disease and eventual death from relapse or disease progression.[7] Therefore, a critical focus in AML therapeutic research is to overcome cellular drug resistance and to develop low-toxicity and highly efficient drugs.

Nanoparticles are defined as particles with at least one dimension less than 100 nanometers. In recent years, nanotechnology has been developing rapidly and is widely used in medical, healthcare, and other related fields. Nanoscale materials have great potential for cancer treatment due to their low risk, fewer complications, and ability to effectively overcome the limitations of conventional drugs, such as reduced bioavailability.[8] Zinc oxide nanoparticles (ZnO NPs) exhibit lower toxicity and higher adsorption capacity than other nanomaterials. And their selective cytotoxicity against cancer cells is 28–35 times higher than that against normal cells.[9] It is also worth noting that ZnO NPs have been approved by the FDA and are widely used in pharmaceutical formulations due to their safety, stability, and biocompatibility.[10] The tumor microenvironment is highly acidic compared to healthy tissue, primarily due to a nearly 200-fold increase in glycolysis and lactic acid production. This results from malignant cellular metabolism, hyperproliferation, and poor perfusion of the tortuous vascular system.[11] Based on the acid-responsive decomposition of ZnO NPs, it can serve as an effective carrier for targeted and sustained delivery of anticancer drugs, effectively promoting cancer cell death and limiting tumor growth.[12] Owing to these features, ZnO NPs are widely used in various biological fields, including antibacterial, anticancer, and disease diagnosis applications.[13–15] Therefore, ZnO NPs can serve as both therapeutic agents and drug carriers for AML treatment, making them a promising option for the development of novel therapies.

Luteolin is a commonly available flavonoid compound found in a wide variety of plants, including fruits, vegetables, and herbs.[16] It has been discovered that luteolin possesses pharmacological properties such as antibacterial and anti-inflammatory effects, as well as the ability to prevent and inhibit the development of various types of tumors and inhibit the invasion and migration of cancer cells, including breast cancer, colon cancer, liver cancer, stomach cancer, and lung cancer.[17–22] Therefore, luteolin has attracted significant attention in cancer therapy due to its broad-spectrum anticancer effects and potential as a natural therapeutic agent.

The possibility of unlimited replication and immortality of tumor cells depends on their success in circumventing cell death regulation. Ferroptosis is a newly discovered cell death type that differs morphologically and physiologically from classical forms of programmed cell death and is primarily driven by lipid peroxidation.[23] Ferroptosis is closely linked to the pathophysiological processes of many diseases, including tumors, neurological disorders, kidney damage, and blood disorders.[24] For example, it was found that when the dihydroartemisinin acts on AML cells, it can accelerate the degradation of ferritin, increase the labile iron pool, promote the accumulation of cellular ROS, and ultimately lead to ferroptosis.[25] Ferroptosis has also been shown to be highly sensitive to drug-resistant cancer cells, especially those in a mesenchymal state and prone to metastasis.[26] Therefore, regulating cellular ferroptosis to influence the development and progression of related diseases has become a major focus of research and therapy. Nanomaterials are recognized by cells as foreign substances and can determine the fate of cells by inducing ferroptosis. For instance, nanoparticles can inhibit the growth and aggressiveness of colorectal cancer cells by stimulating ferroptosis.[27] Additionally, many herb-derived ingredients have been shown to induce ferroptosis in tumor cells. Fu et al demonstrated that luteolin can promote transcription factor EB nuclear translocation and enhances ferritin autophagy in prostate cancer cells, ultimately triggering cellular ferroptosis.[28] Ferroptosis, as a novel mechanism, may play an important role in the treatment of AML.

Luteolin has good anticancer ability, but it cannot be widely used in clinics because of its limited solubility and bioavailability, etc.[29] Unlike the previous studies, which only explored the anti-tumor ability of luteolin and ZnO NPs as a single component, we combined ZnO NPs and luteolin based on the physicochemical properties and excellent drug-carrying capacity of ZnO NPs as well as the excellent anti-tumor ability of luteolin so that it has the functions of both. It can overcome the problem of poor water solubility of luteolin and also be able to target and promote tumor cell death.

In this study, we investigated the induction of ferroptosis by ZnONPs-Lut in the human AML cell line MOLM-13. The present study confirmed that the typical features of ferroptosis–reduced antioxidant defense, accumulation of lipid peroxidation products, and iron overload–were observed in the treated cells. We anticipate that this study will provide a new therapeutic strategy for the treatment of AML.

Materials and Methods

Synthesis of ZnO

ZnO NPs were prepared and synthesized as reported in the relevant papers.[30] ZnO NPs were prepared and synthesized as reported in the relevant literature.30 First, 2.2 g of zinc acetate dihydrate (Sinopharm Chemical Reagent, Shanghai, China) and 0.22 g of magnesium acetate tetrahydrate (Sinopharm Chemical Reagent, Shanghai, China) were dissolved in 60 mL of anhydrous ethanol. The mixture was refluxed under stirring (500 rpm) at 80°C for 2 h until complete dissolution. The solution was then cooled in an ice bath. Next, 0.5 g of NaOH (Sinopharm Chemical Reagent, Shanghai, China) was dissolved in 40 mL of anhydrous ethanol. The solution was subjected to ultrasonication with heating until complete dissolution, followed by cooling in an ice bath. The sodium hydroxide ethanol solution was then added to the ZnO acetate solution in the ice bath. The mixture was stirred at 500 rpm in an ice bath and allowed to react for 4 h to obtain ZnO quantum dots. Finally, 0.5 mL of APTES (Sinopharm Chemical Reagent, Shanghai, China) was mixed with 2 mL of ultrapure water and added to the ZnO quantum dots solution. The mixture was refluxed with stirring (400 rpm) at 60°C for 3 h. A precipitate formed, and the mixture was centrifuged at 7500 rpm for 10 min. The precipitate was collected and washed twice with ethanol to remove unreacted impurities, yielding amino-modified ZnO quantum dots (with lime green fluorescence). Finally, the product was dried under vacuum at room temperature.

Synthesis of ZnONPs-Lut

Luteolin (Sinopharm Chemical Reagent, Shanghai, China) was loaded into ZnO NPs according to the literature.[31] In brief, 0.1 g of ZnO was dispersed in 20 mL of anhydrous ethanol by ultrasonication. Next, 50 mg of luteolin was weighed and dispersed in 10 mL of anhydrous ethanol by ultrasonication. Subsequently, the two solutions were mixed, stirred at room temperature for 12 h, and centrifuged at 7500 rpm for 10 min. The precipitate was washed three times with ethanol to remove unreacted luteolin and then dried under vacuum at room temperature. The loading of luteolin was calculated based on the UV-visible absorbance of luteolin at 351 nm and estimated using a series of calibration curves prepared with luteolin solutions under the same conditions. The drug loading and encapsulation rate were worked out as follows:

$$\text{Drug loading content}\,(\%) = [(\text{weight of drug in nanoparticles})/(\text{weight of drug nanoparticles taken})] * 100\%.$$

$$\text{Drug Entrapment Efficiency}\,(\%) = [(\text{Weight of Drug in Nanoparticles})/(\text{Weight of Drug Injected})] * 100\%$$

Characterization of the Synthesized ZnONPs-Lut

To characterize the synthesized nanoparticles, the crystal structures were analyzed by X-ray diffractometry (XRD; D8 Advance, Bruker, Berlin, Germany). The UV-visible spectra of the nanoparticles were measured using a UV spectrometer (Hitachi U-4100, Hitachi, Tokyo, Japan). The zeta potential and hydrodynamic diameters were measured using a dynamic light scattering (DLS) analyzer (Zetasizer Nano, Malvern Panalytical, UK). The morphology, size, and distribution of ZnONPs-Lut were characterized by transmission electron microscopy (TEM; Tecnai G2 20, FEI, Hillsboro, USA). Additionally, the surface functionalization of ZnONPs-Lut was analyzed using a Fourier transform infrared spectrometer (FTIR; Nicolet 5700, Thermo Nicolet Corporation, MA, USA).

Cells and Cell Culture

The human AML cell line MOLM-13 (Kindly provided by the Hematology Laboratory of Shandong University Qilu Hospital) was incubated in RPMI 1640 (BasalMedia, Shanghai, China) supplemented 10% fetal bovine serum (Sigma, MO, USA), 100 μg/mL streptomycin, and 100 U/mL penicillin. All cells were grown in a 37 °C incubator containing 5% CO_2 air.

Cell Viability Assay

We adjusted log-grown, well-conditioned human AML cells to a cell suspension with a density of 5.0×10^4/mL and evenly inoculated them in 96-well plates (Nest Biotechnology, Wuxi, China). Then, diluted doses of ZnONPs-Lut at

different concentrations (final concentrations of 0, 2.0, 4.0, 8.0, 16.0, 32.0, 64.0, and 128.0 μg/mL) were added to each well. The drug-treated cells were incubated in a sterile incubator at 37 °C for 24 h, 48 h, and 72 h. 20 μL of CCK8 (Elabscience, Wuhan, China) solution was added to each well, and then the cells were further cultured in the incubator for 2 h.[32] Finally, the absorbance of each well was measured at 450 nm.

Real-Time Quantitative PCR (qRT–PCR)

The qRT–PCR was performed to analyze the effects of different concentrations of ZnONPs-Lut (0, 4.0, 8.0, and 16.0 μg/mL) on human AML cells.[33] The mRNA levels of ferroptosis-related genes (ACSL4 and SLC7A11) were measured as target genes, with GAPDH serving as the internal reference. Briefly, MOLM-13 cells were seeded in six-well plates and treated with 0, 4.0, 8.0, and 16.0 μg/mL of ZnONPs-Lut for 24 h. Subsequently, the cells were collected, and total RNA was extracted using the RNA Tissue/Cell Rapid Extraction Kit (Sparkjade Co. Ltd, Shandong, China) according to the manufacturer's instructions. Then, cDNA was synthesized by using a first-strand cDNA synthesis kit (Sparkjade Co. Ltd, Shandong, China). Finally, qRT–PCR was performed using the SPARKScript II SYBR one-step qRT PCR kit (Sparkjade Co. Ltd, Shandong, China). The PCR program was set up as follows: 95 °C for 3 min, then 40 cycles: 95 °C for 5s, 57 °C for 10s, and 72 °C for 15s. The 2-ΔΔCt technique was used to quantify changes in ACSL4 and SLC7A11 mRNA levels after normalization to GAPDH. Primers are listed in Table 1.

Determination of Ferrous Iron(Fe^{2+}) Content, Glutathione (GSH) Content, and Malondialdehyde (MDA)

In this study, a cytosolic ferrous colorimetric test kit (Elabscience, Wuhan, Chinese) was used to measure the amount of Fe^{2+} in human leukemia cell samples.[34] MOLM-13 cells were seeded in six-well plates at a density of 1.0×10^6 cells/well and cultured for 24 h. The MOLM-13 cells were divided into four groups: a control group, an 8.0 μg/mL ZnONPs-Lut group, a 16.0 μg/mL ZnONPs-Lut group, and a 32.0 μg/mL ZnONPs-Lut group. After incubation, the cells were harvested, mixed, and placed on ice for lysis for 10 min. The lysates were then centrifuged at 15,000 × g for 10 min, and the supernatant was collected. The Fe^{2+} levels were determined according to the manufacturer's instructions. For the measurement of GSH, the obtained cells were broken by sonication in an ice bath (200 W power, 3 s pulses with 10s intervals, repeated 30 times), and centrifuged at 12000 g for 10 min. The absorbance at 412 nm of each group was measured according to the instruction of the GSH kit (Solarbio, Beijing, China), and the GSH levels were calculated based on a standard curve.[35] MDA levels in human leukemia cell samples were determined using an MDA colorimetric assay kit (Elabscience, Wuhan, China).[36] After adding the extraction solution, the cells were disrupted using an ultrasonic crusher (90 W, 4 s/time, 2 s gap, total time 10 min) and centrifuged at 10,000 × g for 10 min at 4°C. The samples were incubated in a water bath at 100°C for 40 min, and the absorbance was measured at 532 nm. Protein concentrations were determined using the BCA method, and MDA levels were calculated accordingly.

Reactive Oxygen Species (ROS) Measurement

For ROS measurement, we carried out the experiment by using a reactive oxygen species detection kit containing the fluorescent probe DCFH-DA (Beyotime Biotech, Shanghai, China) and a flow cytometer (NovoCyte, Agilent, CA,

Table 1 Primer Sequences for Gene Expression Analysis

Gene	Primer Sequences
GAPDH	Forward: 5'-GGAAGCTTGTCATCAATGGAAATC Reverse: 5'-TGATGACCCTTTTGGCTCCC
ACSL4	Forward: 5'-CAGAATCATGTGGTGCTGGGAC Reverse: 5'-ATTGTATAACCGCCTTCTTGCC
SLC7A11	Forward: 5'-GGCAGTTGCTGGGCTGATTTA Reverse: 5'-GATGACGAAGCCAATCCCTGT

USA).[37] The intracellular ROS can oxidize non-fluorescent DCFH to produce fluorescent DCF, and the changes in the cellular ROS levels were assessed by measuring DCF fluorescence. Since the fluorescence spectrum of DCF closely resembles that of FITC, we used the same parameter settings as FITC (excitation wavelength: 490 nm; emission wavelength: 520 nm) for the DCF detection.

Mitochondrial Membrane Potential (MMP) Measurement

We employed a flow cytometer (NovoCyte, Agilent, CA, USA) to analyze the changes in intracellular MMP levels according to the manufacturer's instructions for the Mitochondrial Membrane Potential Assay Kit (JC-1) (Beyotime Biotech, Shanghai, China).[38] We used red (excitation wavelength: 525 nm; emission wavelength: 590 nm) and green (excitation wavelength: 490 nm; emission wavelength: 530 nm) fluorochromes to detect JC-1 aggregates and monomers, respectively. The shift from red to green fluorescence of JC-1 was utilized to quantify the reduction in cellular MMP levels.

Western Blot

MOLM-13 cells were divided into the following groups: 0 μg/mL ZnONPs-Lut, 8.0 μg/mL ZnONPs-Lut, 16.0 μg/mL ZnONPs-Lut, 32.0 μg/mL ZnONPs-Lut, 32.0 μg/mL ZnONPs-Lut + DMSO solvent (0.1% DMSO), and 32.0 μg/mL ZnONPs-Lut + ferroptosis inhibitor Ferrostatin-1 (Fer-1; 32.0 μg/mL ZnONPs-Lut + 0.1% DMSO + 1 μmol/L inhibitor; Fer-1 was purchased from MCE, USA, and dissolved in 0.1% DMSO). The protein expression analyzed by Western blot.[39] The whole cells were lysed with RIPA lysis solution, and the protein concentration of each group was quantified using the BCA assay kit (Beyotime Biotech, Shanghai, China). Proteins were denatured for 7 minutes at 100°C. Subsequently, 30 μg of protein was loaded onto a 10% polyacrylamide gel and separated by electrophoresis (30 minutes at 80 V, followed by 120 V until completion). Then, the proteins were transferred onto a polyvinylidene difluoride membrane (90 min, 100 V). The blot was blocked with 5% protein-free rapid blocking buffer (Epizyme Biotech, Shanghai, China) for 30 min. The blocked membrane was incubated overnight at 4°C with the following primary antibodies: ACSL4 (1:6000 dilution; Proteintech, Wuhan, China), GPX4 (1:1000 dilution; Proteintech, Wuhan, China), FTH1 (1:1000 dilution; Cell Signaling Technology, Boston, USA), SLC7A11 (1:1000 dilution; Proteintech, Wuhan, China), and GAPDH (1:2000 dilution; Proteintech, Wuhan, China). The polyvinylidene difluoride membranes were washed with Tris buffered saline Tween (TBS-T; 5 min, 3 times) and incubated with goat anti-rabbit IgG antibody (1:10,000 dilution; Proteintech, China) for 1 h at room temperature. After repeated washing with TBS-T, the protein blot was processed with a chemiluminescence detection kit (Beyotime Biotech, Shanghai, China). Protein quality was estimated with the Typhoon PhosphorImager (GE Healthcare, Piscataway, NJ, USA).

Transmission Electron Microscope (TEM)

The MOLM-13 cells were treated with the varying concentrations of ZnONPs-Lut (0 μg/mL, 8.0 μg/mL, 16.0 μg/mL, 32.0 μg/mL) as well as 32.0 μg/mL ZnONPs-Lut + DMSO solvent, 32.0 μg /mL ZnONPs-Lut + ferroptosis inhibitor in six-well plates for 24 hours. The cells were then centrifuged at 70 g for 5 minutes at room temperature to pellet the cells. The cell pellet was fixed with 2% glutaraldehyde (Solarbio, Beijing, China) for 30 minutes at room temperature under the conditions of light avoidance. The cells were rinsed with 0.1 M phosphate buffer (pH 7.4) for 3 minutes before centrifugation, and this washing step was repeated three times. The 1% agarose solution was prepared by heating, and the cell sediment was picked up with forceps and embedded in agarose after slight cooling. Then, 1% osmium acid (Ted Pella Inc, CA, USA) was used to fix the cells at room temperature for 2 h. After rinsing, the cells were dehydrated through a graded series of ethanol (30%, 50%, 70%, 80%, 95%, and 100%) for 20 minutes each, followed by two 15-minute washes in 100% acetone (Sinopharm Chemical Reagent, Shanghai, China). The ultra-thin sections (60–80 nm) were acquired after infiltrating and embedding of the samples for 48 hours. Finally, the slices were stained with 2% uranyl acetate saturated alcohol solution, 2.6% lead citrate solution, washed, and then dried overnight at room temperature, respectively. The sections were examined using a TEM (Hitachi, Tokyo, Japan), and images were collected for analysis.[40]

Statistical Analysis

The data were analyzed using the IBM SPSS Statistics for Windows, version 28.0 (IBM Corp., Armonk, N.Y., USA), and quantitative data were presented at ± s. Differences between groups were compared by one-way ANOVA, and followed by Dunn's post-hoc test for multiple comparisons. $p < 0.05$ was the threshold for statistical significance.

Results

Characterization of ZnONPs-Lut

Firstly, we prepared the drug ZnONPs-Lut as mentioned in the Methods section. Luteolin was combined with ZnO NPs to facilitate targeted drug delivery to cancer cells. The drug loading capacity (DLC) and drug entrapment efficiency (DEE) were determined to be 16.2% and 32.4%, respectively (Table 2). Then, The size and morphology of ZnONPs-Lut were characterized using TEM, revealing irregular, sphere-like nanoparticles with an average diameter of approximately 4 nm (Figure 1A). Figure 1B shows the XRD graph of synthesized ZnONPs-Lut, where the (102) crystal plane at 34 deg. is not obvious due to the low signal-to-noise ratio. In addition, we performed both fluorescence and UV-Vis spectroscopy to analyze the optical properties of the particles. Figure 1C shows the fluorescence characterization of ZnONPs-Lut and ZnO NPs. Under 350 nm excitation, ZnO NPs exhibited a strong emission peak at approximately 527 nm, whereas ZnONPs-Lut showed no significant emission peak under the same conditions, indicating the presence of some substances in ZnO. The UV-visible absorption spectra of luteolin, ZnO, and ZnONPs-Lut are shown in Figure 1D. Luteolin displayed a strong absorption peak at approximately 351 nm, while the luteolin-loaded ZnO NPs showed reduced intensity at the same wavelength, confirming the successful incorporation of luteolin into the nanoparticles. FTIR spectroscopy further confirmed the surface functionalization of ZnONPs-Lut (Figure 1E). Basically, all the absorption peaks of ZNO can be found in ZnONPs-Lut, with few variations between the two spectra. Through the DLS measurements, we discovered that the average hydrodynamic size of ZnONPs-Lut was 255 nm, which was larger than the size observed by TEM. This discrepancy is attributed to the extensive hydration of the nanoparticles in aqueous solution.[28] The increasing hydrodynamic diameter further supports the successful incorporation of luteolin onto the surface of the ZnO NPs. The zeta potential of ZnONPs-Lut was measured to be 22.1 mV, indicating acceptable colloidal stability.

Cell Viability

To explore the potential influences of ZnONPs-Lut on cell viability, AML cells were treated with a range of ZnONPs-Lut concentrations (0–128.0 μg/mL) for 24 h, 48 h, and 72 h, respectively. The results were shown in Figure 2, ZnONPs-Lut could inhibit the proliferation of MOLM-13 cells in a concentration- and time-dependent manner (*$P < 0.05$, **$P < 0.01$, ***$P < 0.001$ vs relevant control samples). Notably, the IC50 values were 17.1 μg/mL at 24 h, 9.65 μg/mL at 48 h, and 4.73 μg/mL at 72 h. Therefore, we selected 0 μg/mL, 4.0 μg/mL, 8.0 μg/mL, and 16.0 μg/mL for the subsequent experiments.

The qRT–PCR Result

The above experiments had demonstrated that ZnONPs-Lut could indeed cause inhibition of cell viability. To investigate the underlying mechanism and its association with ferroptosis, we analyzed the effect of different doses of ZnONPs-Lut on the expression of ACSL4 and SLC7A11 using qRT–PCR. As shown in Figure 3, treatment of MOLM-13 cells with ZnONPs-Lut led to concentration-dependent changes in the expression of ACSL4 and SLC7A11, with ACSL4 expression increasing (Figure 3A) and SLC7A11 expression decreasing (Figure 3B). (*$P < 0.05$, **$P < 0.01$, and ***$P < 0.001$

Table 2 Drug Loading Content (DLC) and Drug Entrapment Efficiency (DEE) of ZnONPs-Lut

Feed ratio, ZnO: luteolin	DLC%	DEE%
2:1	16.2	32.4

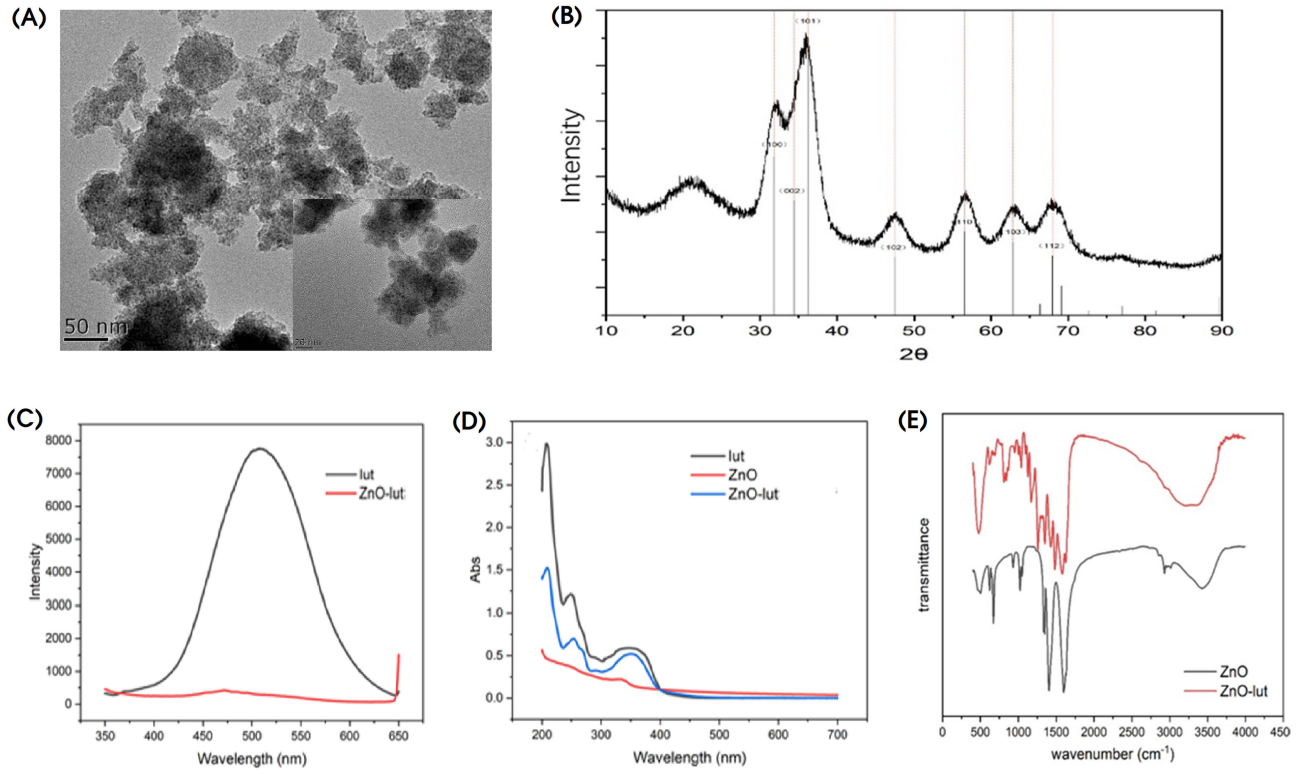

Figure 1 Characterization of ZnONPs-Lut. (**A**) The morphology of ZnONPs-Lut as shown by TEM. (**B**) The X-ray diffraction characterization of ZnONPs-Lut. (**C**) Fluorescence characterization of ZnONPs-Lut and ZnO NPs. (**D**) The UV-vis spectra of luteolin, ZnONPs-Lut, and ZnO NPs. Abs(Absorbance). (**E**) Fourier transform infrared spectra of ZnONPs-Lut, and ZnO NPs.

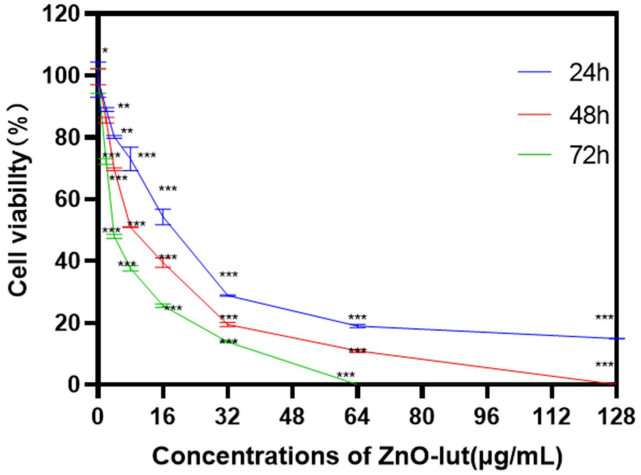

Figure 2 Effects of ZnONPs-Lut on human AML cell viability. MOLM-13 cells were treated with different concentrations (0, 2.0, 4.0, 8.0, 16.0, 32.0, 64.0, and 128.0 μg/ mL) of ZnONPs-Lut for 24 h, 48 h, and 72 h, respectively. And cell viability was tested by the CCK8 method. The results are represented as the mean ± SD (standard deviation) of three independent experiments. *$P < 0.05$, **$P < 0.01$ and ***$P < 0.001$ vs relevant control samples.

compared to control samples). These results revealed that ZnONPs-Lut treatment alters the expression of ferroptosis-related genes compared to the control group, suggesting a close association between AML cell death and ferroptosis. However, ACSL4 expression did not show significant changes at a ZnONPs-Lut concentration of 4 μg/mL, possibly due to the induction of other cell death pathways, such as apoptosis.[16] Therefore, we adjusted the drug concentration to 8.0 μg/mL, 16.0 μg/mL, and 32.0 μg/mL for the smooth running of the subsequent experiments.

https://doi.org/10.2147/IJN.S509007

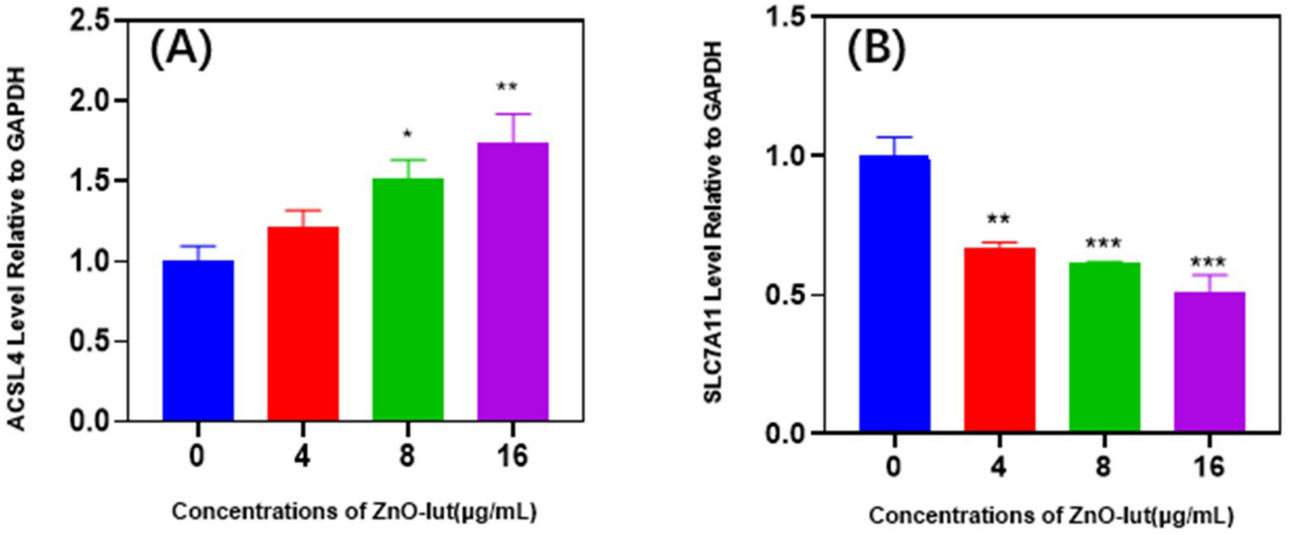

Figure 3 Expression of ACSL4 and SLC7A11 genes. Human AML cells were treated with the varying concentrations of ZnONPs-Lut (0, 4.0, 8.0, and 16.0 μg/mL) for 24 h, and mRNA expression levels of ACSL4 and SLC7A11 were compared to untreated controls. (**A**) ACSL4 mRNA level; (**B**) SLC7A11 mRNA level. Results are presented as mean ± SD of three independent experiments. *$P < 0.05$, **$P < 0.01$ and ***$P < 0.001$ vs relevant control samples.

Intracellular GSH, Fe^{2+}, and MDA Levels

To further investigate the association between proliferation inhibition and ferroptosis, we decided to measure the changes in GSH, Fe^{2+}, and MDA levels in AML cells treated with varying concentrations of ZnONPs-Lut (0 ug/mL, 8.0 μg/mL, 16.0 μg/mL, 32.0 μg/mL). As shown in Figure 4, after 24 h of treatment, GSH levels in MOLM-13 cells decreased in a significant dose-dependent manner (**$p < 0.01$, ***$P < 0.001$ vs control samples), whereas Fe^{2+} and MDA levels rose significantly in a dose-dependent manner. In the present study, it was found that GSH level decreased from 16.19 μg/10^6 cells to 6.30 μg/10^6 cells (Figure 4A). Whereas, Fe^{2+} concentration increased from 0.12 nmol/10^6 to 1.92 nmol/10^6 (Figure 4B), and MDA levels increased from 0.55 nmol/mgprot to 3.60 nmol/mgprot (Figure 4C). These changes are the characteristic of ferroptosis. The results suggest that ZnONPs-Lut may induce ferroptosis in MOLM-13 cells by increasing the level of intracellular Fe^{2+}, inhibiting peroxidase activity, and leading to a decrease of GSH level and accumulation of peroxides in the cells.

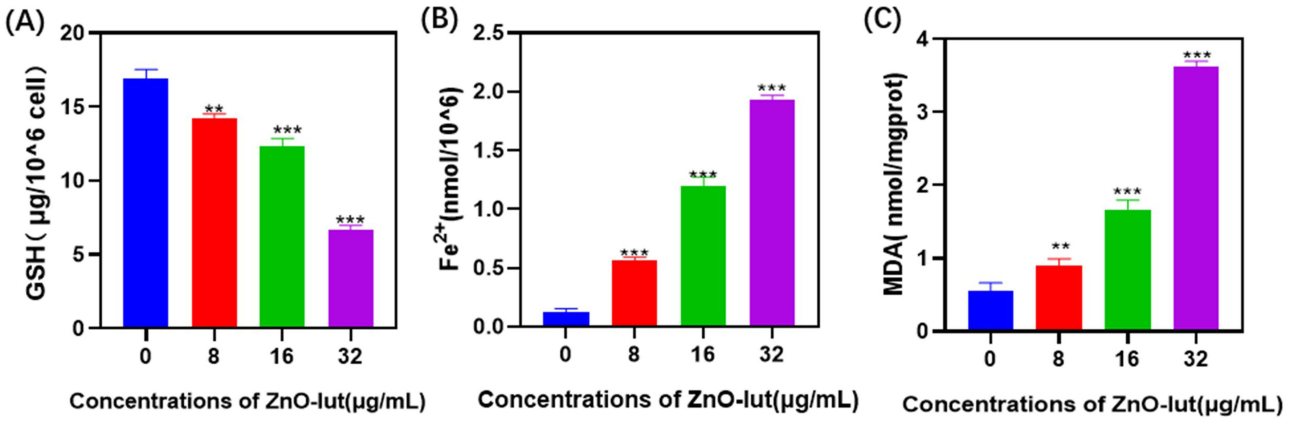

Figure 4 Changes of intracellular GSH, Fe^{2+} and MDA levels in MOLM-13 cells after exposure to different concentrations of ZnONPs-Lut (0, 8.0, 16.0 and 32.0 μg/mL). (**A**) The changes of intracellular GSH levels. (**B**) The changes in intracellular Fe^{2+} levels. (**C**) The changes of intracellular MDA levels. These are three independent experiments. Compared with the control samples, **$P < 0.01$ and ***$P < 0.001$.

Intracellular ROS Level

ROS are one of the key factors of ferroptosis. As shown in Figure 5A-D, the ROS levels in the MOLM-13 cells exhibited an upward trend and showed a concentration-dependent manner when the cells were treated under different concentrations of ZnONPs-Lut. Figure 5E shows that compared to the control group, the ROS levels were significantly enlarged when the cells were exposed to a concentration of 8.0 μg/mL ZnONPs-Lut (**p < 0.01, ***P < 0.001* vs control samples). This result indicates that ZnONPs-Lut could notably induce ROS accumulation in MOLM-13 cells.

Intracellular MMP Levels

As shown in Figure 6A-D, treatment of MOLM-13 cells with ZnONPs-Lut resulted in a significant, concentration-dependent reduction in MMP. Figure 6E demonstrates that exposure to 32.0 μg/mL ZnONPs-Lut significantly reduced intracellular MMP compared to the 8.0 and 16.0 μg/mL treatment groups (**p < 0.01, ***P < 0.001* vs control samples). We speculated that the ZnONPs-Lut-induced cell death pathway might be closely related to mitochondria dysfunction.

GPX4, FTH1, SLC7A11, and ACSL4 Protein Expression

Based on the above experiments, we had initially confirmed that cell death caused by ZnONPs-Lut is closely associated with ferroptosis. To further validate this relationship, we evaluated the expression of ferroptosis-related proteins. And we included a 32.0 μg/mL ZnONPs-Lut + Fer-1 group and a 32.0 μg/mL ZnONPs-Lut + DMSO solvent group alongside the original treatment groups for reverse validation. The results were shown in Figure 7. As shown in Figure 7A, ZnONPs-Lut treatment significantly altered the expression of ferroptosis-related proteins (ACSL4, GPX4, FTH1, and SLC7A11) in MOLM-13 cells. Exposure of MOLM-13 cells to ZnONPs-Lut significantly increased ACSL4 protein expression compared to the control group, while the expression of GPX4, FTH1, and SLC7A11 proteins decreased with increasing ZnONPs-Lut concentration (Figure 7B). In addition, we also observed that, compared to the 32.0 μg/mL ZnONPs-Lut + DMSO group, the 32.0 μg/mL ZnONPs-Lut + Fer-1 group significantly suppressed the increase in ACSL4 expression

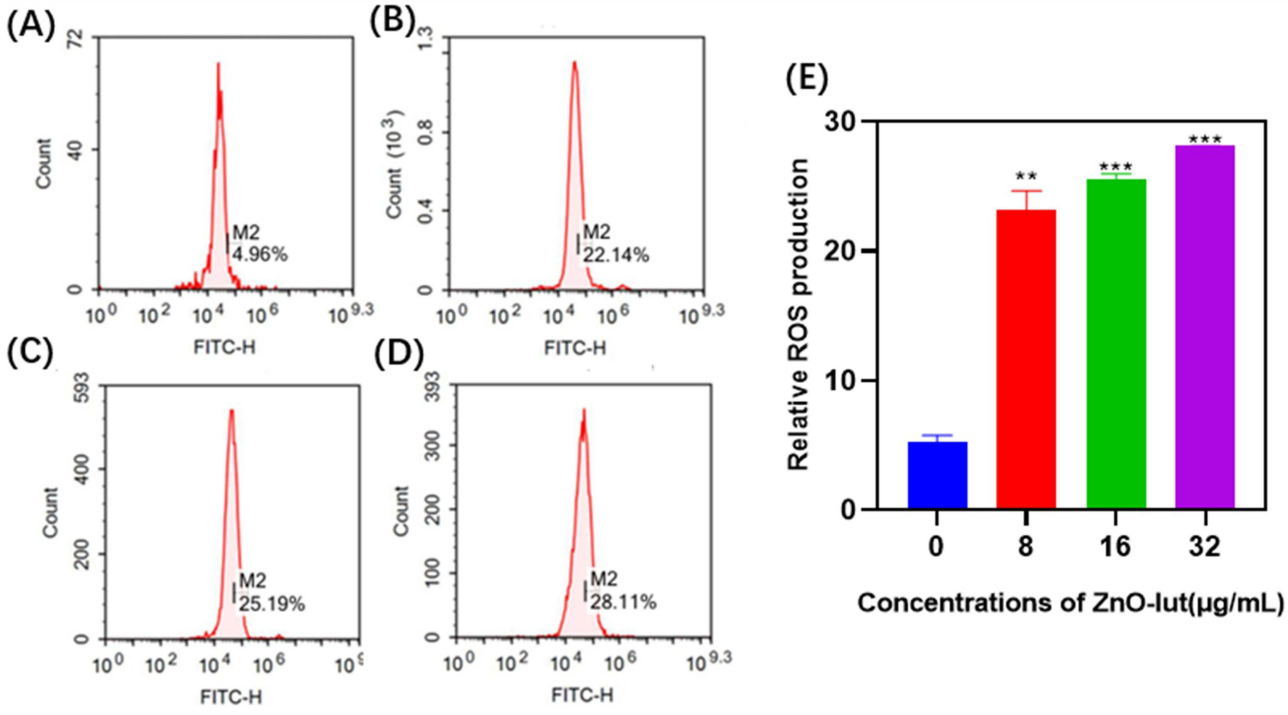

Figure 5 ROS levels in MOLM-13 cells following treatment with varying concentrations of ZnONPs-Lut for 24 hours. (**A–D**) showed ROS levels determined by flow cytometry. (**A**) Untreated MOLM-13 cells. (**B**) MOLM-13 cells treated with 8.0μg/mL ZnONPs-Lut. (**C**) MOLM-13 cells treated with 16.0 μg/mL ZnONPs-Lut. (**D**) MOLM-13 cells treated with 32.0 μg/mL ZnONPs-Lut. (**E**) Histogram analysis of changes in ROS levels after ZnONPs-Lut treatment. Data are from three independent experiments and expressed as mean ± S.D. ***P < 0.01, ***P < 0.001* vs relevant control samples.

https://doi.org/10.2147/IJN.S509007

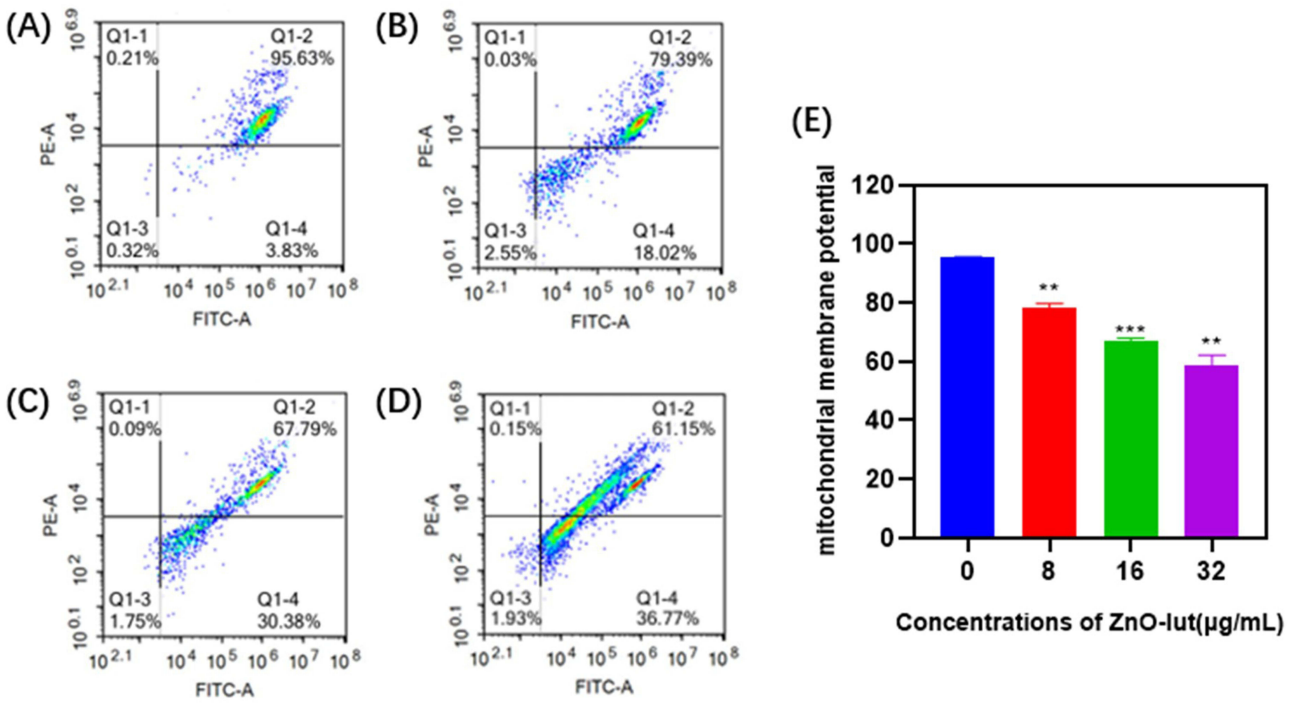

Figure 6 Cellular MMP levels after cells were exposed to different concentrations of ZnONPs-Lut for 24 hours. (**A**) Untreated cells; (**B**) Cells exposed to 8.0 μg/mL ZnONPs-Lut; (**C**) Cells exposed to 16.0 μg/mL ZnONPs-Lut; (**D**) cells exposed to 32.0 μg/mL ZnONPs-Lut. (**E**) The histogram analysis of changes in intracellular MMP under different concentrations of treatments. Data are from three independent experiments. ***P < 0.01*, ****P < 0.001* vs relevant control samples.

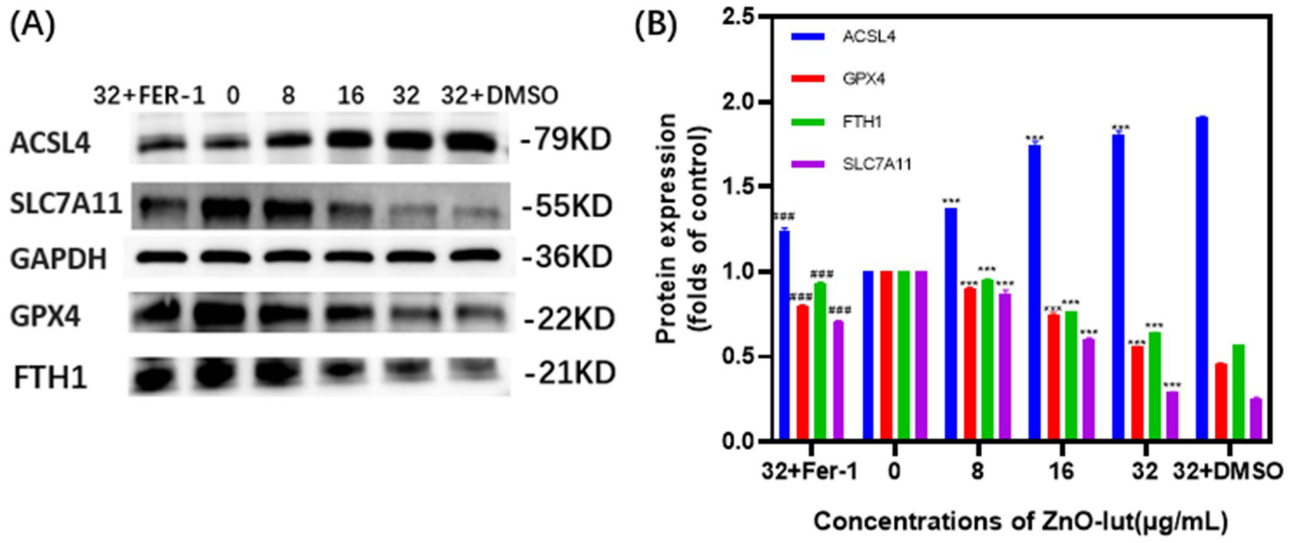

Figure 7 Assessment of protein levels of GPX4, FTH1, SLC7A11 and ACSL4. (**A**) The protein levels of GPX4, FTH1, SLC7A11, ACSL4, and GAPDH in MOLM-13 cells treated with different concentrations of ZnONPs-Lut (0 μg/mL, 8.0 μg/mL, 16.0 μg/mL, 32.0 μg/mL) as well as 32.0 μg/mL ZnONPs-Lut + DMSO solvent, 32.0 μg /mL ZnONPs-Lut + Fer-1 for 24 h and analyzed by Western blot. (**B**) The histogram analysis of target protein expression levels in cells. Data are presented as mean ± SD. ****P < 0.001* vs control samples; *###P < 0.001*, Fer-1 vs DMSO.

and the decrease in GPX4, FTH1, and SLC7A11 expression, thereby inhibiting cellular ferroptosis (Figure 7B). The above findings indicate that all the ferroptosis-related proteins changed significantly after AML cells were exposed to ZnONPs-Lut, and ZnONPs-Lut may induce tumor cell death via the ferroptosis pathway. ****P < 0.001* vs control samples; *###P < 0.001*, Fer-1 vs DMSO).

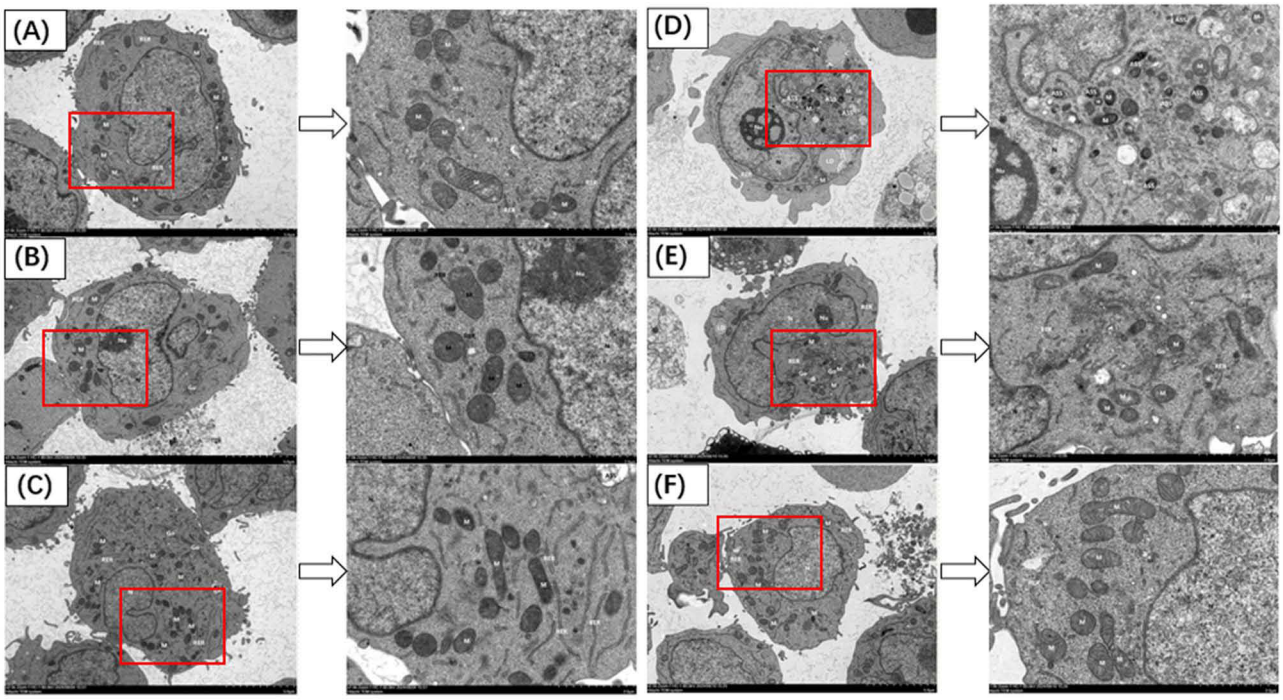

Figure 8 Morphological changes in MOLM-13 cells after 24 hours of treatment. Briefly, the AML cells were treated with different concentrations of ZnONPs-Lut (0, 8.0, 16.0, 32.0 μg/mL), 32 μg/mL ZnONPs-Lut+ 0.1% DMSO, and Fer-1, a ferroptosis inhibitor (32 μg/mL ZnONPs-Lut+ 0.1% DMSO+ 1 μmol/L inhibitor) respectively, followed by observation of cellular morphology using TEM. (**A**) Untreated cells. (**B**) Cells exposed to 8.0μg/mL ZnONPs-Lut; (**C**) Cells exposed to 16 μg/mL ZnONPs-Lut; (**D**) Cells exposed to 32 μg/mL ZnONPs-Lut; (**E**) Cells exposed to 32 μg/mL ZnONPs-Lut and 0.1% DMSO; (**F**) Cells exposed to 32 μg/ mL ZnONPs-Lut, 0.1% DMSO, and 1 μmol/L Fer-1. Nucleus (N); nucleolus (Nu); mitochondria (M); rough endoplasmic reticulum (RERs); lipid droplets (LDs); autophagic lysosomes (ASSs).

The TEM of Cells

The TEM has been widely used to visually assess the states of cells. To further investigate the morphological changes in cells following treatment, we conducted a cellular electron microscopy assay (Figure 8). After 24 hours of treatment with ZnONPs-Lut, MOLM-13 cells exhibited ferroptosis, and the severity of ferroptosis increased in a concentration-dependent manner (Figure 8A-D). At a concentration of 32.0 μg/mL, cell damage was most pronounced. The cells exhibited irregular shapes, intact membranes, and significantly reduced and degraded peripheral microvilli. The intracellular matrix appeared sparse and dissolved, and organelles were visibly solidified, consistent with ferroptosis. The nucleus displayed an irregular shape, with increased heterochromatin and a loosely structured nucleolus. Most mitochondria were significantly wrinkled and smaller, with increased membrane density, high intramembrane electron density, and dilated and reduced cristae. The number of rough endoplasmic reticula decreased, with increased vesicle breaks. Lipid droplets were more abundant, and autophagic lysosomes were present in large numbers. In contrast, compared to the 32.0 μg/mL ZnONPs-Lut + DMSO group, the 32.0 μg/mL ZnONPs-Lut + Fer-1 group significantly inhibited cellular ferroptosis, with most mitochondria displaying intact membranes, parallel cristae, and minimal crumpling and miniaturization (Figure 8E and F). TEM analysis directly demonstrated that ZnONPs-Lut induces ferroptosis in MOLM-13 cells.

Discussion

The element iron is an essential trace element in living organisms. Conversely, iron overload can be cytotoxic. The abnormal accumulation of iron will generate excessive free radicals, which ultimately lead to the damage of DNA, proteins, and other biomolecules. The discovery of ferroptosis explains the pathogenic mechanism of iron overload and also provides a new way to deal with related diseases.[41] Luteolin, an important anticancer agent, has been increasingly reported to contribute to the death of tumor cells and inhibit tumor progression through the cellular ferroptosis mechanism. It has been found that luteolin can enhance oxidative stress in nasopharyngeal carcinoma cells, leading to ferroptosis.[42] Zinc is an essential microelement in the human body, whose oxides exhibit antimicrobial activity at low

https://doi.org/10.2147/IJN.S509007

concentrations. And due to their low toxicity, ZnO NPs are highly effective in the tumor therapy field.[43] Besides the inhibition of tumor cell growth by apoptosis, the anti-tumor effect of ZnO NPs based on ferroptosis has also been identified.[44] Our results showed that MOLM-13 cell viability gradually decreased in a concentration- and time-dependent manner following ZnONPs-Lut treatment. By TEM, we observed the shrinkage of mitochondria in AML cells, characterized by reduced or absent cristae and increased membrane density. These morphological changes are consistent with the features of ferroptosis.[45] All this suggests that ZnONPs-Lut can depress tumor cell viability and promote cell death through ferroptosis mechanism, consistent with previous studies.

Cells can defend against pathogens, including viruses, bacteria, and fungi through regulated cell death such as apoptosis, necrosis, or autophagy.[46] As a newly discovered form of regulated cell death, ferroptosis differs from the classical form of cell death, and is governed by different genes. Oxidative cell necrosis is evoked by overloading of intracellular iron and excessive accumulation of peroxides.[47] The accumulation of lipid peroxides in cells requires iron ions, making ferroptosis an iron-dependent process.[48] The overloaded iron in the iron pool is stored by FTL and FTH1. Treatment of AML cells with ZnONPs-Lut reduced FTH1 expression, decreasing iron storage capacity, increasing intracellular iron levels, and ultimately inducing ferroptosis.[49] It has been found that lipid metabolism is closely related to ferroptosis, with iron-dependent lipid ROS accumulation playing a central role in the ferroptosis pathway.[50] The changes of the MDA content in cells, an indicator of lipid peroxidation, are also closely associated with ferroptosis.[51] Under iron overload conditions, the ACSL4, as a promoter of ferroptosis, is overexpressed, promoting the conversion of polyunsaturated fatty acids to polyunsaturated fatty acid phospholipids (PUFA-PLs) in cells and decreasing MMP.[52–54] The excess PUFA-PLs are peroxidized in the presence of ROS generated by the Fenton reaction, leading to the disruption of the lipid bilayer membranes of the cells and ultimately to ferroptosis.[55,56] These findings align with our experimental results. The SLC7A11 is a core regulator of ferroptosis, which can modulate the sensitivity of cancer cells to ferroptosis mainly through the SLC7A11/GSH/GPX4 axis.[57] In this study, we found that the expression of SLC7A11 was positively correlated with the GPX4 and GSH levels. We reviewed the literature and found that inhibition of SLC7A11 transcription and expression reduces GSH levels, suppressing GPX4 activity, leading to ROS accumulation, increased cellular sensitivity to ferroptosis, and ultimately promoting ferroptosis.[58] Thus, all of our experimental results indicated that ZnONPs-Lut can promote ferroptosis in MOLM-13 cells. The specific mechanism is illustrated in Figure 9. To further validate these findings, we added the Fer-1 treatment group, which reversed the expression levels of ferroptosis-related

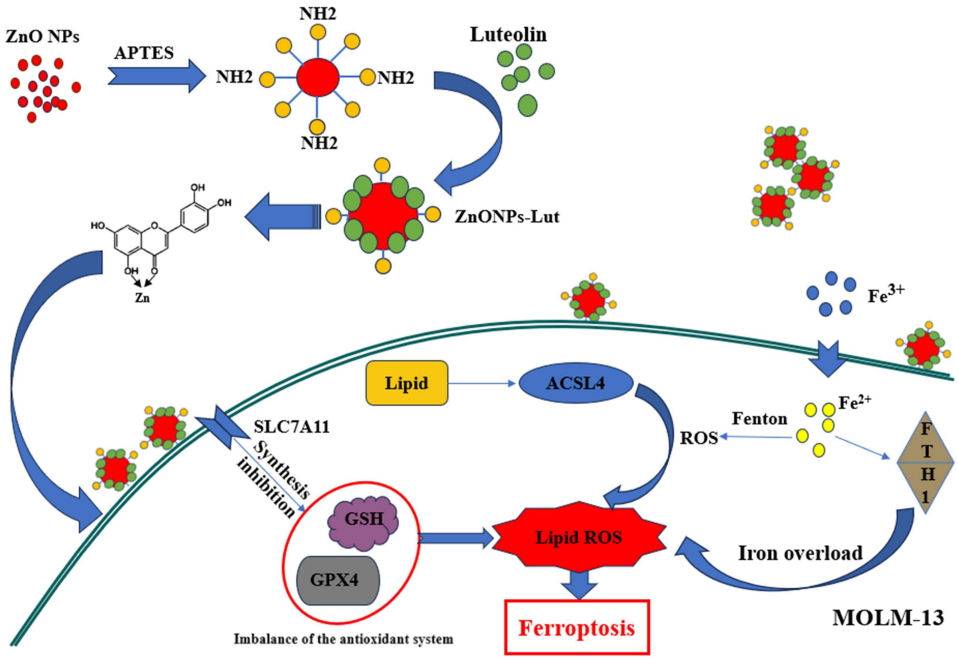

Figure 9 Schematic illustration of ZnONPs-Lut-induced ferroptosis in the AML cell line MOLM-13.

proteins and restored cellular structures associated with ferroptosis, as observed by electron microscopy. This reverse validation confirms that the drug can inhibit cell proliferation by promoting ferroptosis in MOLM-13 cells, which may provide potential evidence for the development of anticancer drugs.

The clinical treatment of relapsed and refractory AML remains a significant challenge in hematology, primarily due to drug resistance in tumor cells, which drives disease recurrence and treatment failure. Therefore, overcoming the drug resistance of tumor cells is the key factor to solve the problem of AML recurrence. It has been found that tumor drug resistance may be closely connected with ferroptosis. The tumor cells may raise intracellular GSH and inhibit ROS production through a variety of mechanisms, leading to drug resistance and tumor recurrence.[59] Based on this inference, ferroptosis is a cell death pathway independent of tumor cell drug resistance mechanisms. As an excellent ferroptosis inducer, ZnONPs-Lut can bypass the drug resistance mechanisms of AML cells and directly induce tumor cell death. Additionally, unlike traditional chemotherapy drugs, which can cause long-term damage to vital organs such as the heart,[60] both ZnO NPs and luteolin exhibit low toxicity, making them suitable for long-term disease treatment.[9,16] Furthermore, ZnONPs-Lut, as a combination of ZnO NPs and luteolin, retains the functional properties of both components. It retains the multi-target capabilities of luteolin, including cell cycle inhibition, apoptosis induction, angiogenesis suppression, and tumor progression blockade.[61] It also benefits from the drug delivery capabilities of ZnO NPs, enhancing drug targeting and bioavailability while reducing damage to normal tissues.[62] Luteolin exhibits significant antioxidant and anti-inflammatory effects, which can mitigate oxidative stress and inflammatory responses caused by chemotherapy drugs.[63] Thus, ZnONPs-Lut can serve as a complementary therapy to traditional chemotherapy, reducing its adverse effects.

In the present experiments, we were the first to synthesize a new compound, ZnONPs-Lut, and investigate its effect on ferroptosis in MOLM-13 cells. As a spherical nanoparticle with a diameter of approximately 4 nm, ZnONPs-Lut likely possesses additional features and capabilities that warrant further exploration. Compared with rod-shaped nanoparticles, its spherical structure has more advantages such as higher absorption rates and increased cellular uptake efficiency.[64] In addition, the smaller the size of the nanoparticle, the better its capacity to navigate through the tumor interstitium. Due to its small size, ZnONPs-Lut can penetrate deeper into tumor tissues and be excreted via the kidneys, minimizing toxic side effects.[65] Further improvements are possible, such as finding the optimal reactant concentrations by concentration gradient experiments to improve the synthesis efficiency, or modifying the nanoparticle surface (eg PEGylation) to prolong the blood circulation time and enhance the therapeutic effect.[66] And we believe that ZnONPs-Lut has the potential to serve as a foundation for developing novel therapeutic agents for leukemia.

Conclusion

We conducted an initial investigation into the relationship between ZnONPs-Lut and ferroptosis in MOLM-13 cells, exploring the underlying molecular mechanisms. However, there were limitations in our study. Our experiments were conducted only in one cell line, MOLM-13, and were not demonstrated in the animal models. Additionally, the related signaling pathways were not further investigated. Our results showed that ZnONPs-Lut effectively inhibited the proliferation and promoted the death of MOLM-13 cells in a dose- and time-dependent manner. ZnONPs-Lut effectively increased Fe^{2+} and MDA levels, decreased the expression levels of GSH and MMP, and induced the generation of ROS in MOLM-13 cells. In addition, ZnONPs-Lut also significantly up-regulated ACSL4 protein expression while down-regulated GPX4, FTH1, and SLC7A11 protein expression compared to the control group, thereby activating the ferroptosis signaling pathway. Moreover, Fer-1, a ferroptosis inhibitor, effectively suppressed the ZnONPs-Lut-induced ferroptosis. In summary, our findings indicate that ZnONPs-Lut induces ferroptosis in AML cells, thereby inhibiting their proliferation.

Abbreviations

AML, Acute myeloid leukemia; ZnONPs-Lut Zinc oxide nanoparticles-luteolin; GSH, Glutathione; MMP, Mitochondrial membrane potential; MDA, Malondialdehyde; ROS, Reactive oxygen species; Fer-1, Ferrostatin-1; TEM, Transmission electron microscopy; ZnO NPs, Zinc oxide nanoparticles; Fe^{2+}, Ferrous iron; QRT–PCR Real-Time Quantitative PCR;

XRD, X-ray diffractometry; DLS Dynamic light scattering; FTIR, Fourier transform infrared; PUFA-PLs, Polyunsaturated fatty acid phospholipids.

Data Sharing Statement

Data sharing is not applicable to this article as no datasets were generated or analysed during the current study.

Acknowledgments

The authors gratefully acknowledge the key projects supported by the Natural Science Foundation of China (82374237). We gratefully acknowledge Jinan Guoke Medical Technology Development Co., Ltd. for their technical expertise in preparing zinc oxide nanoparticles-luteolin composites.

Author Contributions

All authors made a significant contribution to the work reported, whether that is in the conception, study design, execution, acquisition of data, analysis and interpretation, or in all these areas; took part in drafting, revising or critically reviewing the article; gave final approval of the version to be published; have agreed on the journal to which the article has been submitted; and agree to be accountable for all aspects of the work.

Funding

This work was supported by the National Natural Science Foundation of China (82374237).

Disclosure

The authors declare that they have no competing interests.

References

1. Park S, Cho BS, Kim HJ. New agents in acute myeloid leukemia (AML). *Blood Res*. 2020;55(S1):S14–S18. doi:10.5045/br.2020.S003
2. Shimony S, Stahl M, Stone RM. Acute myeloid leukemia: 2023 update on diagnosis, risk-stratification, and management. *Am J Hematol*. 2023;98(3):502–526. doi:10.1002/ajh.26822
3. SEER*Explorer. An interactive website for SEER cancer statistics [Internet]. Bethesda: Surveillance Research Program, National Cancer Institute; 2024. M04 17. [updated: 2024 M11 5; cited 2025 M02 10]. Available from: https://seer.cancer.gov/statistics-network/explorer/. Accessed March 28, 2025.
4. Liu H. Emerging agents and regimens for AML. *J hematol oncol*. 2021;14(1):49.
5. Shao R, Li Z, Xin H, et al. Biomarkers as targets for CAR-T/NK cell therapy in AML. *Biomark Res*. 2023;11(1):65. doi:10.1186/s40364-023-00501-9
6. Gale RP. Can Immune Therapy Cure Acute Myeloid Leukemia? *Curr Treat Options Oncol*. 2023;24(5):381–386. doi:10.1007/s11864-023-01066-3
7. Mohamed Jiffry MZ, Kloss R, Ahmed-Khan M, et al. A review of treatment options employed in relapsed/refractory AML. *Hematology*. 2023;28(1):2196482. doi:10.1080/16078454.2023.2196482
8. Anjum S, Hashim M, Malik SA, et al. Recent advances in zinc oxide nanoparticles (ZnO NPs) for cancer diagnosis, target drug delivery, and treatment. *Cancers (Basel)*. 2021;13(18):4570. doi:10.3390/cancers13184570
9. Alipour S, Babaei G, Gholizadeh-Ghaleh Aziz S, Abolhasani S. Alantolactone and ZnO nanoparticles induce apoptosis activity of cisplatin in an ovarian cancer cell line (SKOV3). *Res Pharm Sci*. 2022;17(3):294–304. doi:10.4103/1735-5362.343083
10. Li Z, Yin X, Lyu C, et al. Zinc oxide nanoparticles trigger autophagy in the human multiple myeloma cell line RPMI8226: an in vitro study. *Biol Trace Elem Res*. 2024;202(3):913–926. doi:10.1007/s12011-023-03737-6
11. Ratnam M, Hao H, Zheng X, et al. Receptor induction and targeted drug delivery: a new antileukaemia strategy. *Expert Opin Biol Ther*. 2003;3(4):563–574. doi:10.1517/14712598.3.4.563
12. Feng Y, Yang W, Shi X, Zhao X. ZnO-incorporated alginate assemblies: tunable pH-responsiveness and improved drug delivery for cancer therapy. *Int J Biol Macromol*. 2024;255:128189. doi:10.1016/j.ijbiomac.2023.128189
13. Villegas-Fuentes A, Rosillo-de la Torre A, Vilchis-Nestor AR, Luque PA. Improvement of the optical, photocatalytic and antibacterial properties of ZnO semiconductor nanoparticles using different pepper aqueous extracts. *Chemosphere*. 2023;339:139577. doi:10.1016/j.chemosphere.2023.139577
14. Yang R, Wu R, Mei J, Hu FR, Lei CJ. Zinc oxide nanoparticles promotes liver cancer cell apoptosis through inducing autophagy and promoting p53. *Eur Rev Med Pharmacol Sci*. 2021;25(3):1557–1563. doi:10.26355/eurrev_202102_24864
15. Ibraheem S, Kadhim AA, Kadhim KA, Kadhim IA, Jabir M. Zinc oxide nanoparticles as diagnostic tool for cancer cells. *Int J Biomater*. 2022;2022:2807644. doi:10.1155/2022/2807644
16. Lin Y, Shi R, Wang X, Shen HM. Luteolin, a flavonoi d with potential for cancer prevention and therapy. *Curr Cancer Drug Targets*. 2008;8(7):634–646. doi:10.2174/156800908786241050

17. Rakoczy K, Kaczor J, Sołtyk A, et al. Application of Luteolin in Neoplasms and Nonneoplastic Diseases. *Int J mol Sci*. 2023;24(21):15995. doi:10.3390/ijms242115995
18. Wu HT, Lin J, Liu YE, et al. Luteolin suppresses androgen receptor-positive triple-negative breast cancer cell proliferation and metastasis by epigenetic regulation of MMP9 expression via the AKT/mTOR signaling pathway. *Phytomedicine*. 2021;81:153437. doi:10.1016/j.phymed.2020.153437
19. Yoo HS, Won SB, Kwon YH. Luteolin induces apoptosis and autophagy in HCT116 colon cancer cells via p53-dependent pathway. *Nutr Cancer*. 2022;74(2):677–686. doi:10.1080/01635581.2021.1903947
20. Rath P, Chauhan A, Ranjan A, et al. *Luteolin: A Promising Modulator of Apoptosis and Survival Signaling in Liver Cancer*. Pathol Res Pract.
21. Yajie D, Feng L, Zhaoyan LI, et al. Efficacy of luteolin on the human gastric cancer cell line MKN45 and underlying mechanism. *J Tradit Chin Med*. 2023;43(1):34–41. doi:10.19852/j.cnki.jtcm.2023.01.005
22. Masraksa W, Tanasawet S, Hutamekalin P, Wongtawatchai T, Sukketsiri W. Luteolin attenuates migration and invasion of lung cancer cells via suppressing focal adhesion kinase and non-receptor tyrosine kinase signaling pathway. *Nutr Res Pract*. 2020;14(2):127–133. doi:10.4162/nrp.2020.14.2.127
23. Zhao L, Zhou X, Xie F, et al. Ferroptosis in cancer and cancer immunotherapy. *Cancer Commun (Lond)*. 2022;42(2):88–116. doi:10.1002/cac2.12250
24. Li J, Cao F, Yin HL, et al. Ferroptosis: past, present and future. *Cell Death Dis*. 2020;11(2):88. doi:10.1038/s41419-020-2298-2
25. Du J, Wang T, Li Y, et al. DHA inhibits proliferation and induces ferroptosis of leukemia cells through autophagy dependent degradation of ferritin. *Free Radic Biol Med*. 2019;131:356–369. doi:10.1016/j.freeradbiomed.2018.12.011
26. Jiang X, Stockwell BR, Conrad M. Ferroptosis: mechanisms, biology and role in disease. *Nat Rev mol Cell Biol*. 2021;22(4):266–282. doi:10.1038/s41580-020-00324-8
27. Zhang Z, Zhao Y, Wang Y, Zhao Y, Guo J. Autophagy/ferroptosis in colorectal cancer: carcinogenic view and nanoparticle-mediated cell death regulation. *Environ Res*. 2023;238(Pt 2):117006. doi:10.1016/j.envres.2023.117006
28. Fu W, Xu L, Chen Y, et al. Luteolin induces ferroptosis in prostate cancer cells by promoting TFEB nuclear translocation and increasing ferritinophagy. *Prostate*. 2024;84(3):223–236. doi:10.1002/pros.24642
29. Chen L, Chang S, Zhao L, et al. Biosynthesis of a water solubility-enhanced succinyl glucoside derivative of luteolin and its neuroprotective effect. *Microb Biotechnol*. 2022;15(9):2401–2410. doi:10.1111/1751-7915.14095
30. Muhammad F, Guo M, Qi W, et al. pH-Triggered controlled drug release from mesoporous silica nanoparticles via intracellular dissolution of ZnO nanolids. *J Am Chem Soc*. 2011;133(23):8778–8781. doi:10.1021/ja200328s
31. Sadhukhan P, Kundu M, Chatterjee S, et al. Targeted delivery of quercetin via pH-responsive zinc oxide nanoparticles for breast cancer therapy. *Mater Sci Eng C Mater Biol Appl*. 2019;100:129–140. doi:10.1016/j.msec.2019.02.096
32. Liu J, Jia S, Yang Y, et al. Exercise induced meteorin-like protects chondrocytes against inflammation and pyroptosis in osteoarthritis by inhibiting PI3K/Akt/NF-κB and NLRP3/caspase-1/GSDMD signaling. *Biomed Pharmacother*. 2023;158:114118. doi:10.1016/j.biopha.2022.114118
33. Matsuda N, Sato S, Shiba K, et al. PINK1 stabilized by mitochondrial depolarization recruits Parkin to damaged mitochondria and activates latent Parkin for mitophagy. *J Cell Biol*. 2010;189(2):211–221. doi:10.1083/jcb.200910140
34. Bartolini D, Arato I, Mancuso F, et al. Melatonin modulates Nrf2 activity to protect porcine pre-pubertal Sertoli cells from the abnormal H_2O_2 generation and reductive stress effects of cadmium. *J Pineal Res*. 2022;73(1):e12806. doi:10.1111/jpi.12806
35. Alpert AJ, Gilbert HF. Detection of oxidized and reduced glutathione with a recycling postcolumn reaction. *Anal Biochem*. 1985;144(2):553–562. doi:10.1016/0003-2697(85)90153-8
36. Yang Z, Wang J, Ai S, Sun J, Mai X, Guan W. Self-generating oxygen enhanced mitochondrion-targeted photodynamic therapy for tumor treatment with hypoxia scavenging. *Theranostics*. 2019;9(23):6809–6823. doi:10.7150/thno.36988
37. Alsagaby SA. Transcriptomics-based investigation of molecular mechanisms underlying apoptosis induced by ZnO nanoparticles in human diffuse large B-cell lymphoma. *Int J Nanomed*. 2022;17:2261–2281. doi:10.2147/IJN.S355408
38. Li X, Chen M, Yang Z, Wang W, Lin H, Xu S. Selenoprotein S silencing triggers mouse hepatoma cells apoptosis and necrosis involving in intracellular calcium imbalance and ROS-mPTP-ATP. *Biochim Biophys Acta Gen Subj*. 2018;1862(10):2113–2123. doi:10.1016/j.bbagen.2018.07.005
39. Yin J, Guo J, Zhang Q, et al. Doxorubicin-induced mitophagy and mitochondrial damage is associated with dysregulation of the PINK1/parkin pathway. *Toxicol In Vitro*. 2018;51:1–10. doi:10.1016/j.tiv.2018.05.001
40. Zhang J, Qin X, Wang B, et al. Zinc oxide nanoparticles harness autophagy to induce cell death in lung epithelial cells. *Cell Death Dis*. 2017;8(7):e2954. doi:10.1038/cddis.2017.337
41. Zager RA. Parenteral iron compounds: potent oxidants but mainstays of anemia management in chronic renal disease. *Clin J Am Soc Nephrol*. 2006;1 Suppl 1:S24–31.
42. Wu Z, Qu Q. Mechanism of luteolin induces ferroptosis in nasopharyngeal carcinoma cells. *J Toxicol Sci*. 2024;49(9):399–408. doi:10.2131/jts.49.399
43. Yin X, Li Z, Lyu C, et al. Induced effect of zinc oxide nanoparticles on human acute myeloid leukemia cell apoptosis by regulating mitochondrial division. *IUBMB Life*. 2022;74(6):519–531. doi:10.1002/iub.2615
44. Ashoub MH, Amiri M, Fatemi A, Farsinejad A. Evaluation of ferroptosis-based anti-leukemic activities of ZnO nanoparticles synthesized by a green route against Pre-B acute lymphoblastic leukemia cells (Nalm-6 and REH). *Heliyon*. 2024;10(17):e36608. doi:10.1016/j.heliyon.2024.e36608
45. Gao W, Wang X, Zhou Y, Wang X, Yu Y. Autophagy, ferroptosis, pyroptosis, and necroptosis in tumor immunotherapy. *Signal Transduct Target Ther*. 2022;7(1):196. doi:10.1038/s41392-022-01046-3
46. Gao J, Wang Q, Tang YD, Zhai J, Hu W, Zheng C. When ferroptosis meets pathogenic infections. *Trends Microbiol*. 2023;31(5):468–479. doi:10.1016/j.tim.2022.11.006
47. Dixon SJ, Lemberg KM, Lamprecht MR, et al. Ferroptosis: an iron-dependent form of nonapoptotic cell death. *Cell*. 2012;149(5):1060–1072. doi:10.1016/j.cell.2012.03.042
48. Yan B, Ai Y, Sun Q, et al. Membrane damage during ferroptosis is caused by oxidation of phospholipids catalyzed by the oxidoreductases POR and CYB5R1. *Mol Cell*. 2021;81(2):355–369.e10. doi:10.1016/j.molcel.2020.11.024

49. Manz DH, Blanchette NL, Paul BT, Torti FM, Torti SV. Iron and cancer: recent insights. *Ann N Y Acad Sci*. 2016;1368(1):149–161. doi:10.1111/nyas.13008
50. Park E, Chung SW. ROS-mediated autophagy increases intracellular iron levels and ferroptosis by ferritin and transferrin receptor regulation. *Cell Death Dis*. 2019;10(11):822. doi:10.1038/s41419-019-2064-5
51. Tsikas D. Assessment of lipid peroxidation by measuring malondialdehyde (MDA) and relatives in biological samples: analytical and biological challenges. *Anal Biochem*. 2017;524:13–30. doi:10.1016/j.ab.2016.10.021
52. Wang Y, Zhang M, Bi R, et al. ACSL4 deficiency confers protection against ferroptosis-mediated acute kidney injury. *Redox Biol*. 2022;51:102262. doi:10.1016/j.redox.2022.102262
53. Doll S, Proneth B, Tyurina YY, et al. ACSL4 dictates ferroptosis sensitivity by shaping cellular lipid composition. *Nat Chem Biol*. 2017;13(1):91–98. doi:10.1038/nchembio.2239
54. Chen GH, Song CC, Pantopoulos K, Wei XL, Zheng H, Luo Z. Mitochondrial oxidative stress mediated Fe-induced ferroptosis via the NRF2-ARE pathway. *Free Radic Biol Med*. 2022;180:95–107. doi:10.1016/j.freeradbiomed.2022.01.012
55. Lei G, Zhuang L, Gan B. Targeting ferroptosis as a vulnerability in cancer. *Nat Rev Cancer*. 2022;22(7):381–396. doi:10.1038/s41568-022-00459-0
56. Zou Y, Henry WS, Ricq EL, et al. Plasticity of ether lipids promotes ferroptosis susceptibility and evasion. *Nature*. 2020;585:7826):603–608.
57. Ye Y, Chen A, Li L, et al. Repression of the antiporter SLC7A11/glutathione/glutathione peroxidase 4 axis drives ferroptosis of vascular smooth muscle cells to facilitate vascular calcification. *Kidney Int*. 2022;102(6):1259–1275. doi:10.1016/j.kint.2022.07.034
58. Chu B, Kon N, Chen D, et al. ALOX12 is required for p53-mediated tumour suppression through a distinct ferroptosis pathway. *Nat Cell Biol*. 2019;21(5):579–591. doi:10.1038/s41556-019-0305-6
59. Galadari S, Rahman A, Pallichankandy S, Thayyullathil F. Reactive oxygen species and cancer paradox: to promote or to suppress? *Free Radic Biol Med*. 2017;104:144–164. doi:10.1016/j.freeradbiomed.2017.01.004
60. Moudgil R, Yeh ET. Mechanisms of cardiotoxicity of cancer chemotherapeutic agents: cardiomyopathy and beyond. *Can J Cardiol*. 2016;32(7):863–870.e5. doi:10.1016/j.cjca.2016.01.027
61. Tuorkey MJ. Molecular targets of luteolin in cancer. *Eur J Cancer Prev*. 2016;25(1):65–76. doi:10.1097/CEJ.0000000000000128
62. Wang J, Lee JS, Kim D, Zhu L. Exploration of zinc oxide nanoparticles as a multitarget and multifunctional anticancer nanomedicine. *ACS Appl Mater Interfaces*. 2017;9(46):39971–39984. doi:10.1021/acsami.7b11219
63. López-Lázaro M. Distribution and biological activities of the flavonoid luteolin. *Mini Rev Med Chem*. 2009;9(1):31–59. doi:10.2174/138955709787001712
64. Chithrani BD, Ghazani AA, Chan WC. Determining the size and shape dependence of gold nanoparticle uptake into mammalian cells. *Nano Lett*. 2006;6(4):662–668. doi:10.1021/nl052396o
65. Albanese A, Tang PS, Chan WC. The effect of nanoparticle size, shape, and surface chemistry on biological systems. *Annu Rev Biomed Eng*. 2012;14(1):1–16. doi:10.1146/annurev-bioeng-071811-150124
66. Rahme K, Dagher N. Chemistry Routes for Copolymer Synthesis Containing PEG for Targeting, Imaging, and Drug Delivery Purposes. *Pharmaceutics*. 2019;11(7):327. doi:10.3390/pharmaceutics11070327